18TH WORLD CONFERENCE ON EARTHQUAKE ENGINEERING
WCEE2024
MILAN

MILAN, ITALY
30TH JUNE - 5TH JULY 2024

www.wcee2024.it

PUSHOVER ANALYSES OF ROCKING-SLIDING MASONRY WALLS USING MACRO-ELEMENT AND RIGID MACRO-BLOCK MODELS

L. Giresini[1], B. Pantò[2] & C. Casapulla[3]

[1] University La Sapienza, Rome, Italy

[2] University of Durham, Durham, UK

[3] University of Naples Federico II, Naples, Italy

Abstract: *Historical and monumental masonry constructions are generally vulnerable to out-of-plane failures due to the absence of rigid floors and poor connections between orthogonal walls. This leads to activating rocking mechanisms of external walls or façades, whose ultimate force and displacement are affected by a complex dynamic structural behaviour between the rocking façade and transverse walls. This interaction is often neglected in the engineering practice. However, this simplified assumption may lead to significant approximations, as demonstrated by numerous experimental and numerical studies in the literature. This paper investigates the rocking capacity of unreinforced masonry walls interacting with adjacent transverse walls and subjected to out-of-plane loadings. Interlocking effects are simulated through frictional resistances according to the macro-block model (MBM) used for macro-limit analysis. Based on the equivalence of the contiunuous distribution of these forces and the discrete distribution of transversal elastic-plastic links, a numerical model is developed by using the discrete macro-element method (DMEM), starting from the onset of the failure mechanism and during its evolution. The results of the two models are compared in terms of both force-displacement and pushover curves, with reference to the case study of a front wall of a two-storey unreinforced masonry building. The presented preliminary results demonstrate the capability of the DMEM to describe the load and displacement capacities of rocking walls accounting for the contribution of lateral walls. Although the paper focuses on a specific case study, the presented results allow for assessing the contribution of lateral walls in the stage of activation and during the evolution of the rocking mechanism and can represent a base for the definition of more accurate procedures for assessing local failures of historic masonry buildings.*

1. Introduction

The seismic assessment of existing masonry buildings is based on a two-level approach, regarding local and global analyses. Local analysis is carried out to verify all the possible out-of-plane (OOP) mechanisms of the building, while the global one is based on the building box-type behaviour, where in-plane (IP) failures of walls are involved. The analysis of OOP mechanisms is of fundamental importance especially for historic or old buildings or arch-type structures (Andreini et al. 2013, Ferreira et al. 2015), either not seismically designed or designed with obsolete seismic standards. These modes are generally analysed by performing either force-based or displacement-based approaches (Sorrentino et al. 2017), using kinematic analyses (Degli Abbati et al. 2021, Casapulla et al. 2021) or dynamic analyses (AlShawa et al. 2023, Coccia and Como 2023, Giresini et al. 2021a).

For what regards kinematic analyses of simple rocking walls, the basic model first proposed by Heyman (1966) was properly extended to include interlocking effects due to friction with transverse walls, both at the onset

(Casapulla 2001) and during the evolution of the rocking mechanism (Casapulla and Argiento 2016), through the implementation of the so-called macro-block model (MBM). The related formulation for the frictional resistances was then adopted by the Italian seismic codes (MIT 2019) and the MBM was further extended to non-regular masonry patterns by Szabó et al. 2022 and by Funari et al. 2022.

For what concerns dynamic analyses, approaches considering rigid-block models connected to transverse walls, tie-rods, vaults, or energy dissipation devices were recently developed also including fragilities (Nale et al. 2023, Giresini 2022, Jaimes et al. 2021). Among these boundary conditions, it is confirmed that the most important ones are the transverse walls, as they are always present in buildings and do participate in their seismic performance. Referring to rigid-block models, the role of transverse walls is considered by either assuming a modified coefficient of restitution (Sorrentino et al. 2011) or explicitly accounting for a rigid or for an elastic contact (Alshawa et al. 2023, Giresini et al. 2021b).

Nevertheless, the dynamics of rigid-block motion is affected by some limitations, not considering masonry deformability, three-dimensional wall boundary conditions and complex failure mechanisms other than simple overturning or horizontal/vertical bending. That is why more sophisticated approaches were established making use of discrete macro-element (DMEM), distinct element (DEM) and detailed finite element (FEM) methods. Among them, the DMEM is characterized by a very low computational cost compared to DEM and FEM. Moreover, for masonry buildings this method presents many advantages if compared to the others, related to geometrical consistency, possibility to combine discrete and finite elements, straightforward model calibration, possibility to be used at macro and meso-scale (Vadalà et al. 2022). Recently, the DMEM was enriched by considering P-delta effects through a standard iterative Newton-Raphson method implemented in the commercial engineering-oriented HiStrA software package (Cusmano et al. 2023). The introduction of geometric nonlinearities was validated through numerical and experimental results available in the literature demonstrating its capacity to describe the nonlinear response of rocking masonry walls subjected to different boundary and loading conditions.

However, apart from some implementations at micro/meso scale, especially with DEM (Chen and Bagi 2020, Pulatsu et al. 2022, Orosz and Bagi 2023) and FEM (Pepe et al. 2020, Yavartanoo and Kang 2022), interlocking effects of walls with their transverse walls are still not properly simulated in the modelling approaches with low computational effort, although it is well recognised that this phenomenon plays a relevant role both at the onset and during the evolution of local failure mechanisms. An original contribution in this line is the attempt to convert the analytical frictional resistances proposed by Casapulla and Argiento (2016) in an equivalent tensile unitary stiffness of a spring bed connected to the dynamic rigid-block model (Casapulla et al. 2017). Two possible choices to define the equivalent tensile stiffness were discussed in that work: the first one consists of considering the ultimate displacement of the constant frictional resistance *plateau*, occurring between the activation of motion and the first loss of contact in the units, whilst the second one assumes a mean displacement value in the range of the subsequent decreasing frictional resistances, due to the progressive detachment of courses. However, only the elastic behaviour of the springs was assumed and the frictional resistances were not considered in their evolution, so the state of art still requires a more sophisticated approach.

This paper, therefore, proposes the implementation of the masonry wall interlocking within a refined DME model by means of a vertical distribution of elastic-plastic links, based on the original analytical representations of the frictional resistances as continuous variables at the onset and during the evolution of the simple rocking. Section 2 illustrates the frictional model with its implications in a pushover analysis of a rocking wall. In Section 3, the interaction between a masonry façade and lateral walls is simulated by a discrete lateral distribution of nonlinear links defined within the DMEM strategy. Section 4 discusses pushover analyses applied to a front wall of a two-storey unreinforced masonry building.

2. Simulation of the wall interlocking using the macro-block model

2.1 Frictional model for simulating interlocking with continuous formulations

The refined macro-block model (MBM) suitable for analysing local mechanisms in multi-storey unreinforced masonry buildings (Casapulla et al. 2021) is herein used to develop continuous formulations for the interlocking between two orthogonal walls based on frictional resistances. In particular, only the simple rocking-sliding

mechanism of the front wall under horizontal actions is considered here, with cogged cracks close to the connections with the side walls, generally simulating weak connections (Fig. 1b).

According to the concept of macro-modelling, it is assumed that these cogged cracks, one per side wall, separate the structure into two macro blocks (the moving front wall and the resting side walls), and all the possible relative motions among micro blocks (units) are concentrated along them. Masonry block walls with regular units and staggering (single-leaf walls arranged in a running bond pattern) are assumed, where the macro blocks and the constituent units have infinite strength in compression, tension and shear, while no-tension and frictional behaviour is assumed at their contact interfaces along the cracks (Coulomb failure criterion). The latter assumption can be used to simulate the interlocking between the front and orthogonal walls based on frictional forces, as described by Casapulla (2001) and then adopted by the Commentary to the Italian technical standards, namely CNTC19 (MIT 2019), with a formulation of the resultant frictional resistance here rearranged as (Fig. 1b):

$$F = \sum_{1}^{n} S_i = \frac{n(n+1)}{2} v h t_s \gamma_s f = \frac{n(n+1)}{2} W_b f \qquad (1)$$

In this equation, n is the number of courses in the side wall crossed by the crack, γ_s is the specific weight of the side walls, f is the friction coefficient, and t_s, h and $v = l/2$ are the width (assumed equal to the side-wall thickness), the height and the overlapping length of the unit, respectively, as sketched in Fig. 1a. Note that W_b is the weight of a single half-unit (Figs. 1a and 1b) and CNTC19 suggests a reduction by 20% of Eq. (1) to account for rocking-sliding motion.

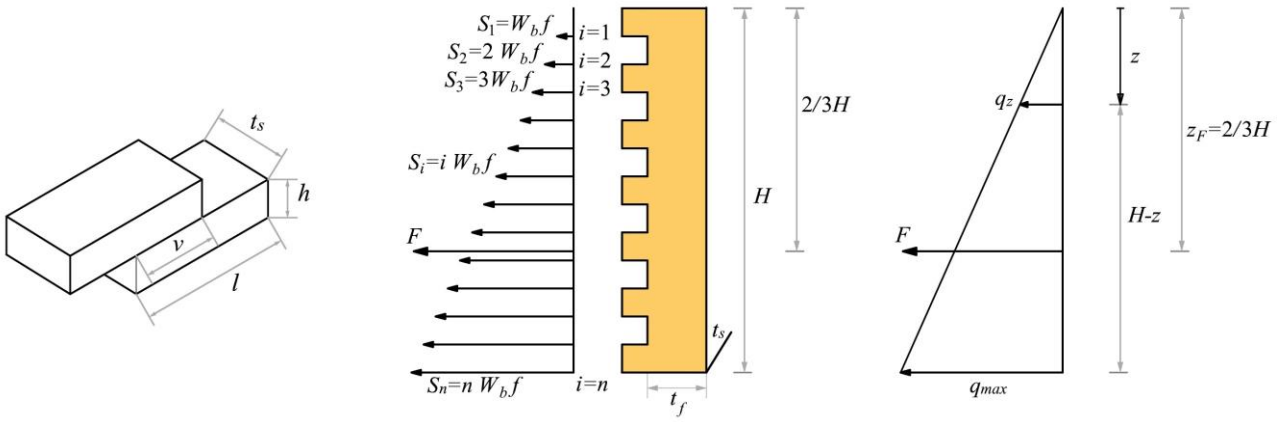

Figure 1. MBM. a) Masonry unit dimensions; b) frictional resistances transmitted to the front wall (in yellow colour) by the side walls along the vertical cogged crack; c) linear representation of the frictional resistances.

As shown in Fig. 1b, the value of the frictional force at each bed joint linearly increases with the height of the side wall from the top, with the application point of their resultant at 2/3 of the total height. Based on that, Eq. (1) can be expressed through the continuous variable q_z, being z the variable height from the top, as (Fig. 1c):

$$F = \int_0^H q_z \, d_z = \frac{H \, q_{max}}{2} \qquad (2)$$

from which, known F, q_z and the application point of its resultant z_F can be derived as:

$$q_z = \frac{z}{H} q_{max} = \frac{2F}{H^2} z$$
$$z_F = \frac{\int_0^H (q_z \, z \, d_z)}{F} = \frac{2}{3} H \qquad (3)$$

The continuous formulations in Eq. (3) allow discretizing the frictional resistances as a number of elastic-plastic springs with their own stiffness, as described in Section 3.

2.2 Pushover analysis for the simple rocking-sliding mechanism of masonry walls

The simple rocking-sliding mechanism of the front wall is a mechanism that does not involve the side walls and the crack pattern can be actually identified *a priori*. The mechanism triggers when the front wall starts rotating around its external bottom edge (ideally a cylindrical hinge), while the units along the two cogged cracks exhibit a rocking-sliding motion with a clear prevalence of sliding.

The evolution of this mechanism after the formation of the hinge strictly depends on the frictional forces, which gradually reduce after a certain displacement, due to the progressive loss of contact in the units along the cracks. The variation of these forces can be represented by nonlinear (step) functions of the displacement, as originally developed within the MBM by Casapulla and Argiento (2016) and briefly described in the following.

The effectiveness of these forces calculated by Eq. (1) on the whole height H of each side wall is guaranteed as long as the first two courses at its top lose their contact with the fixed portion of the wall along the crack (first threshold displacement). As the wall rotation increases, the subsequent threshold displacements are assumed to be attained at every two underlying courses of the front wall that lose the contact with the side wall. This means that, considering the generic detached course i in Fig. 2, the threshold displacement is reached when $dx_i = v$, i.e. when the overlapping of units is lost at the distance from the base equal to (r_i h), being r_i the number of courses still involved in frictional contact as:

$$r_i = n - i \qquad i = 0,2,4,\dots,n \tag{4}$$

Thus, it will be:

$$dx_{Gi} = \frac{nv}{2r_i} \tag{5}$$

while the corresponding reduced frictional resistance F_i can be easily calculated by replacing n with r_i, in Eq. (1), i.e.:

$$F_i = \frac{r_i(r_i + 1)}{2} W_b f \tag{6}$$

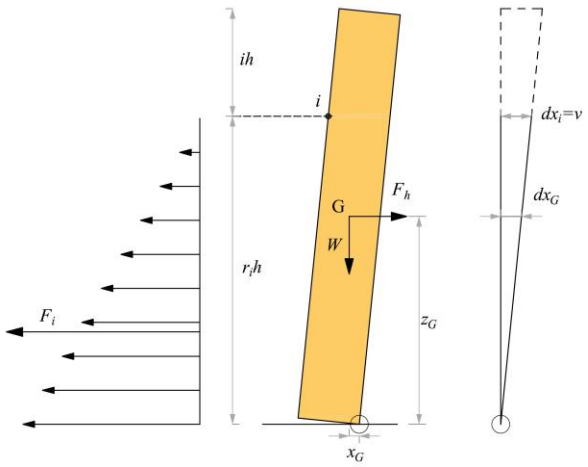

Figure 2. MBM. Variation of frictional resistances at increasing wall rotation.

Then, nonlinear kinematic analysis allows investigating the evolution of the mechanism till collapse through a pushover curve, which relates the horizontal load F_h to the horizontal displacement of the front wall centre of gravity d_{xG}, assumed as the control point. The curve can be obtained by applying the theorem of virtual works, considering varied kinematic configurations of the examined mechanism, at large displacements, as (Fig. 3):

$$F_h(\vartheta) = \frac{W x_G(\vartheta) + 2F z_F(\vartheta)}{z_G(\vartheta)} \tag{7}$$

where ϑ is the finite rotation, while the horizontal displacement of the control point will be:

$$dx_G(\vartheta) = \frac{t_f}{2} - x_G(\vartheta) \tag{8}$$

It is worth noting that *F* in Eq. (7) follows the variability of Eq. (6) and that at the onset of the mechanism ($\vartheta = 0$) F_h has its maximum value, as sketched for the pushover curves developed for the case study in Section 4.

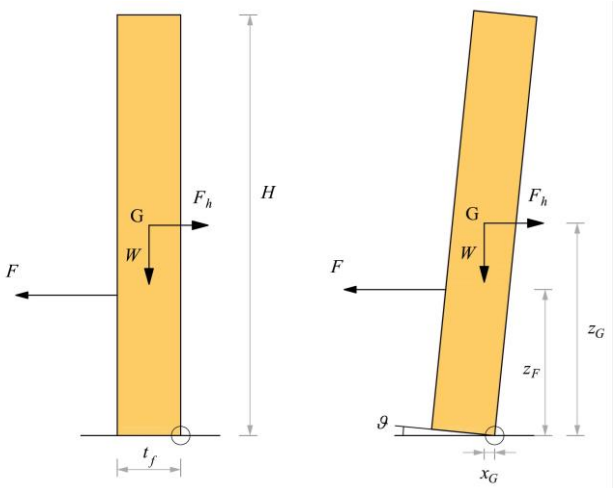

a) b)

Figure 3. MBM. a) Initial and b) varied kinematic configurations of the rocking front wall.

3. Implementation within the macro-element model

The DMEM strategy consists in discretising a masonry wall by a mesh of shear-deformable spatial macro-elements (Fig. 4a) connected to the other elements through nonlinear zero-thickness interfaces (Fig. 4b). Each macro-element is governed by seven degrees of freedom describing the six independent rigid motions (U, V, W, Φ, Ψ, Θ) of the element and one parameter (γ) representing the element shear deformation. Each interface comprises a set of nonlinear mono-dimensional links calibrated by performing straightforward equivalences between the continuum material and the equivalent discrete model (Pantò et al. 2017; Chácara et al. 2019).

The number of orthogonal links is generally chosen according to the desired level of accuracy to be reached for the interface integration. It is worth noting that no additional Lagrangian parameters are needed to describe the kinematics of interfaces. In this study, the links describing the sliding at the base interface of the front wall are kept elastic and sufficiently rigid, while the transversal links, governing the base partialisation of the same wall, are considered elastic in compression and with zero tensile strength. The DMEM P-Delta formulation recently proposed by Cusmano et al. (2023) is employed in this study to perform the analyses.

According to this strategy, the geometrical nonlinearities are considered by updating the current positions of the external and along-interface internal forces applied to the macro-elements. This simplified procedure avoids assembling and updating the geometrical stiffness matrix according to the current system configuration, ensuring good efficiency of the model. More details on the model formulation and validation can be found in Caliò et al. (2012) and Pantò et al. (2017).

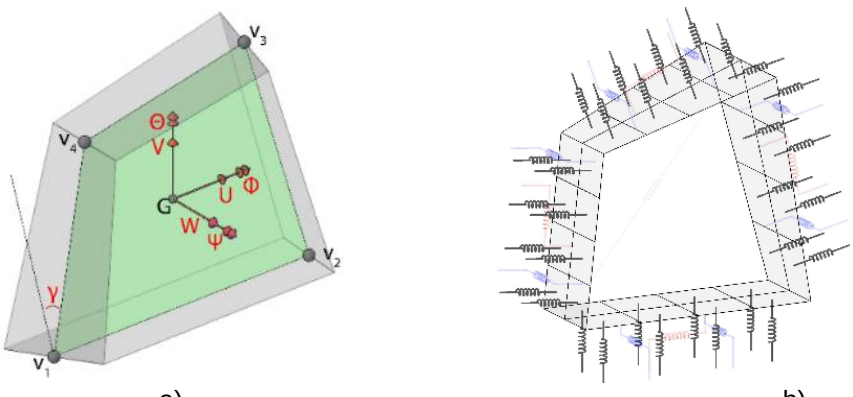

a) b)

Figure 4. DMEM. a) Lagrangian parameters of the macro-element; b) interface nonlinear links.

3.1 Interlocking simulation

Based on the frictional model (MBM) described in Section 2, the interaction between masonry façade and side walls can be implemented within the DMEM through a discrete lateral distribution of 1D nonlinear links, herein called *interlocking links*, each describing some brick courses (two courses in Fig. 5a). The mechanical behaviour of each of these links is characterised by an initial stiffness (*K*), an ultimate force (F_u), and an ultimate displacement (d_u), as displayed in Fig. 5d. The ultimate force of the generic *j*-th link is expressed as:

$$F_{u,j} = q_{z,j}\, 2h_L \tag{9}$$

where $q_{z,j}$ is the distributed frictional force per unit length at z_j, given by the first of Eq. (3), and h_L is the area represented by the link. The equivalence between the continuous function of the frictional resistances in Fig. 1c (expressed by Eq. (1)) and their discrete variation (provided by Eq. (9)) is displayed in Fig. 5b, where the linear and the stepped functions are overlapped. The ultimate displacement ($d_{u,j}$) of the generic *j*-th interlocking link is associated with the loss of support at the bottom section of the area represented by the link, whose distance from the top of the wall can be expressed as $z_j + h_L/2$. It results:

$$d_{u,j} = \frac{l}{2}\frac{H - z_j}{H - (z_j + \frac{h_L}{2})} \tag{10}$$

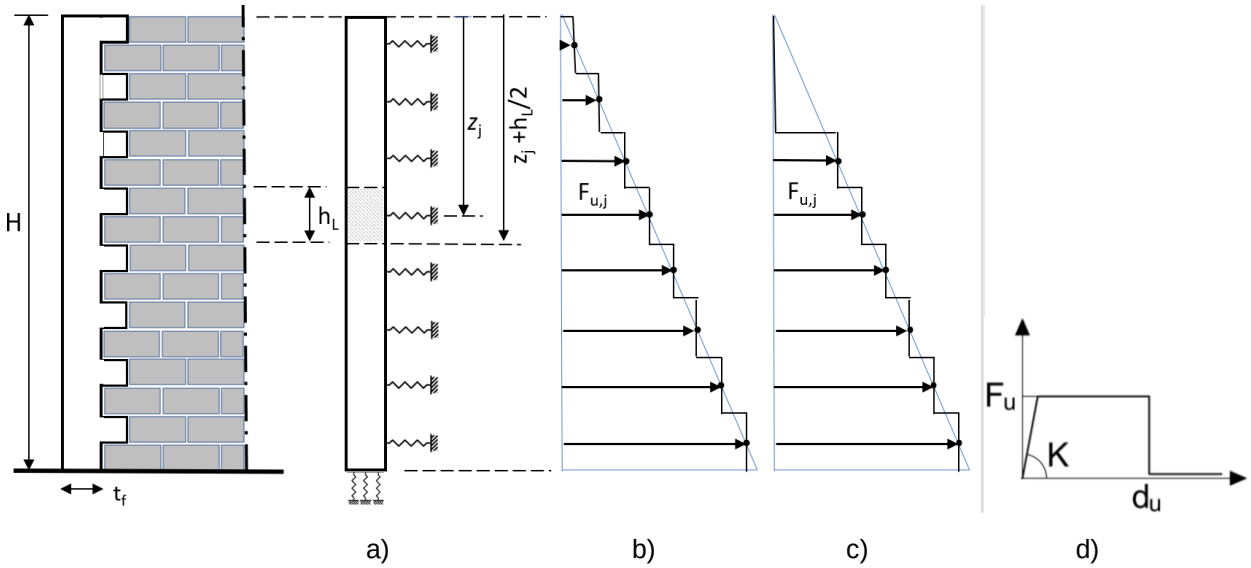

Figure 5. DMEM. a) Discrete link distribution simulating interlocking between walls; overlapping of the frictional resistance distributions for the DMEM (stepped line) and the MBM (continuous line) in the cases of b) all links active and c) loss of support at the first two links; d) constitutive law of each nonlinear link.

where l is the width of the bricks (Fig. 1a). Finally, the elastic stiffness (*K*) is evaluated considering a displacement of 0.1 mm when the link reaches the ultimate force. This value is arbitrarily assumed to simulate a quasi-rigid behaviour of the interlocking link before the sliding activation.

3.2 Pushover analysis

The pushover analyses within the DMEM framework are performed by considering an incremental process where an external force is applied to the barycentric point of the wall. At each step of the analysis, the stiffness matrix and the load vector are updated to take into account the nonlinearities of the interface links and the geometric nonlinearities (P-Delta effects). At each step, the equilibrium is reached by an iterative Newton-Raphson procedure with an arch-length control method to follow the softening branch of the capacity curve.

The mechanism is activated when the first row of transversal links of the interface at the base of the wall goes in tension and progresses until only one row remains in compression. This corresponds to the rotation of the front wall around a clindrical hinge not at the external edge but very close to it. On the other hand, in the stage when all the interlocking links are active ($d_j \leq d_{u,j}$), the resistant forces of these links approximate the triangular distribution of the continuous, as shown in Fig. 5b, where the black lines indicate the forces corresponding to

the links of the DMEM and the blue line the force distribution corresponding to the MBM. Finally, the force of each interlocking link drops to zero as the link reaches the ultimate displacement, and the force of the link is redistributed to the other links, as represented by the MBM in Fig. 2. In the DMEM, instead, the stabilising weight of the masonry column above each considered sliding interface is not updated at the failure of each link. As a result, the links provide the trapezia force distribution illustrated in Fig. 5c, where the adapted curve for the MBM is also reported with the continuous blue line. It represents a simplified hypothesis of the DMEM whose effects on the global displacement capacity of the wall will be evaluated in the next section and will be the object of future upgrades of the model. From the physical point of view, this hypothesis can be considered representative of a possible scenario in which the cracks between the façade and the lateral walls are not perfectly vertical, involving a portion of lateral walls in the mechanism, continuing to provide the stabilising weight against friction sliding.

4. Results and discussions

The front wall of a two-storey unreinforced masonry building analysed by Galvez et al. (2021) in the OOP behaviour using the discrete element modelling (DEM) approach is considered in this section as an application example of the two models described in the previous sections. This building is inspired by one of the benchmark studies investigated within the Italian ReLUIS III research project on Masonry Structures (Cattari and Magenes 2021), mostly focused on their global behaviour rather than on the local failure modes.

The wall geometry is the same as that indicated by Galvez et al. (2021), which was slightly modified in the thickness and without including openings with respect to the original one, as sketched in Fig. 6b.

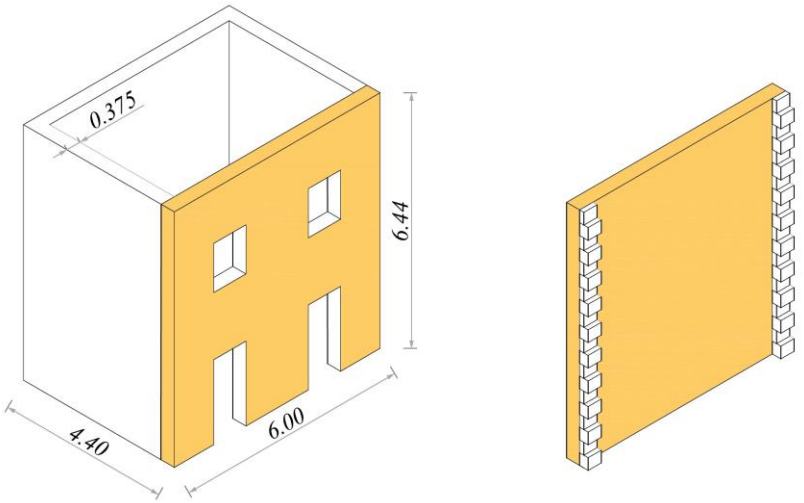

a) b)

Figure 6. Geometrical model of the two-storey case study building. a) Units in m; b) front wall without openings but with indentations with the side walls.

The elements representing the interlocking between the front and the side walls are 20 courses of bricks with adapted dimensions of 0.25 × 0.322 × 0.375 m^3 (l × h × t_s), arranged in a running bond pattern, while the friction coefficient is assumed to be f = 0.577.

Using the MBM with Eqs. (5) and (6), the frictional resistance-displacement curve referred to the control point of the front wall centre of gravity and to the contribution of both side walls is reported as a dashed red line in Fig. 7a, highlighting its reduction as the wall rotation increases after the first threshold displacement dx_G = 0.07m. The related pushover curve according to Eqs. (7) and (8) is displayed in Fig. 7b, together with the case of the isolated front wall (no interlocking), represented by the grey continuous line. In particular, the first linear descending branch of the dashed red pushover curve is characterised by the effectiveness of frictional resistances acting on the whole height of the corners, till when these values start to reduce in correspondence with the first threshold displacement given by Eq. (5) with i = 2. Considering the effective vertical cracks at the wall corners, the subsequent nonlinear reduction of frictional forces represented by Eq. (6) implies a linear descending step function of F_h, with different measures of the risers and treads. In fact, it

is worth noting that the increasing displacement of the control point involves longer descending branches and shorter heights of the steps due to the more displacement capacity associated with the lower part of the corners with respect to the upper one and lower frictional resistances, respectively. Instead, if the stabilising weight of the masonry column above each sliding interface continues to be considered at the failure of each link, as in the DMEM, the first risers are smaller than the subsequent ones, so representing sub-vertical cracks (continuous red line in Fig. 7).

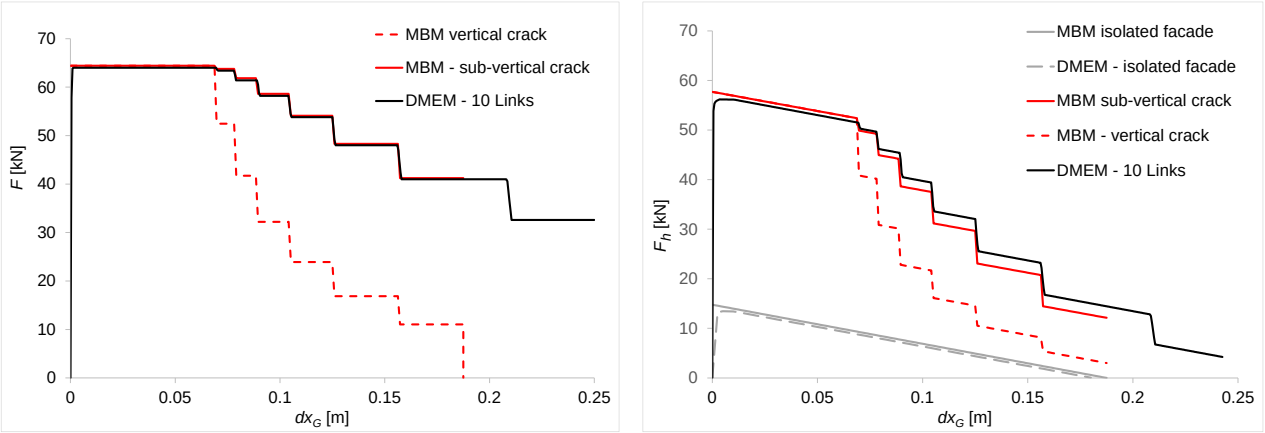

a) b)

Figure 7. MBM. a) Frictional resistance-displacement curves and b) pushover curves with reference to the front wall centre of gravity and the contribution of both side walls.

Using the DMEM, three different interlocking link discretisations are adopted: ten links (one link every two brick courses), five links (one link every four brick courses), and a single link. The calibration of the stiffnesses and the application points of the links belonging to any distribution must follow the equivalence with the continuous distribution of the MBM (Fig. 1c), in terms of both resultant force and moment. So, in the cases of ten and five links, each link is located at the barycentre of the link contact area, as represented in Fig. 5a, and the link ultimate displacement is evaluated considering the sliding section coincident with the below section of the link area. When a single link is adopted, it is located at 1/3 height from the base to guarantee the same ultimate moment of the continuous MBM, and the link ultimate displacement is conventionally evaluated considering the sliding section at H/2 (Table 1).

The results of the analyses are shown in Fig. 7, comparing the MBM and the refined DMEM in terms of frictional resistances (Fig. 7a), and external force (Fig. 7b) vs. the front wall centre of gravity. The results for the isolated wall are also reported in Fig. 7b for comparison to evaluate the role of frictional resistances.

It can be observed that considering the hypothesis of sub-vertical cracks, the results predicted by the two models are coincident, while, modelling the failure mechanism characterised by a vertical crack, the DMEM leads to an overestimation of the system displacement capacity. Future upgrades of the DMEM, and in particular the constitutive law of the interlocking links (Fig. 5d) need to be considered to cover this current limitation of the DMEM to allow it to simulate a vertical crack and mixed mechanisms. Finally, some differences can be observed with the results obtained by Galvez et al. (2021), not reported in the graphs. These may be justified by the fact that different constitutive laws characterise the DEM, but this will be the object of further investigations and comparisons.

Finally, a parametric analysis is conducted by varying the number of the interlocking links disposed along with the height of the wall, calibrated as described above. The results, shown in Fig. 8, evidence that the model with 10 and 5 links provides very similar responses, while the model with a single link provides a reasonable description of the system until a lateral displacement of 0.1m (approximative 40% of the critical displacement). The latter result is promising in using the single-link DMEM for practical applications and assessments, where the limit of 40% is identified as the ultimate limit performance level by CNTC19 (MIT, 2019).

Table 1. Calibration of the DMEM links.

j	z_j	$z_j + 0.5h_L$	$F_{u,j}$	$d_{u,j}$	K_j
	m	m	kN	m	kN/m
10 links					
1	0.324	0.648	0.322	0.132	3220
2	0.972	1.296	0.966	0.133	9661
3	1.620	1.944	1.610	0.134	16102
4	2.268	2.592	2.254	0.135	22543
5	2.916	3.240	2.898	0.138	28984
6	3.564	3.888	3.543	0.141	35425
7	4.212	4.536	4.187	0.146	41866
8	4.860	5.184	4.831	0.156	48307
9	5.508	5.832	5.475	0.188	54748
10	6.156	6.480	6.119	-	61189
5 links					
1	0.648	1.296	1.288	0.141	12882
2	1.944	2.592	3.865	0.146	38646
3	3.240	3.888	6.441	0.156	64409
4	4.536	5.184	9.017	0.188	90173
5	5.832	6.480	11.594	-	115937
1 link					
1	4.320	3.240	32.205	0.083	322047

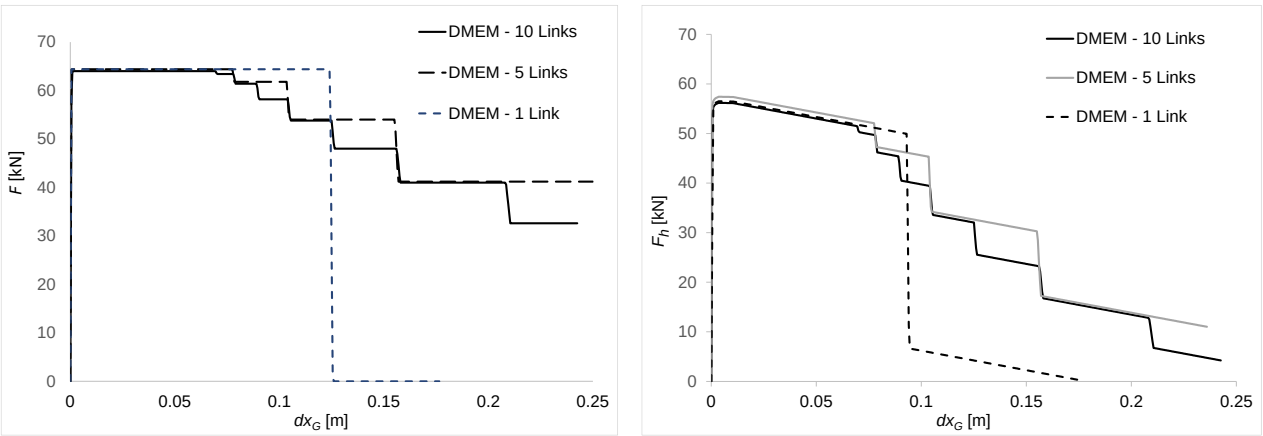

a) b)

Figure 8. DMEM. a) Frictional resistance-displacement curves and b) pushover curves for different link discretisations.

5. Conclusions

The paper presents a new implementation within the discrete macro-element method (DMEM) to describe the interaction between rocking masonry walls and lateral walls. These interlocking effects are simulated through frictional resistances according to the macro-block model (MBM) used for macro-limit analysis. Based on the equivalence of the contiunuous distribution of these forces and the discrete distribution of transversal elastic-plastic links, a refined DMEM is developed to simulate the onset of the rocking-sliding mechanism and its evolution. The model accuracy is evaluated by performing pushover analyses and comparing the results against those obtained by the MBM, both in terms of frictional forces and pushover capacity curves. The results

evidence good consistency between the DMEM and the MBM till the first first loss of contact in the units, while they suggest the need for future improvements of the DMEM to simulate the mechanism with vertical cracks.

In the last part of the paper, the influence of the number of the interlocking links on the wall response is investigated. The results of parametric analyses evidence the capability of the DMEM in employing a single link to simulate the lateral response of the wall until a limit of approximately 40% of the critical displacement, making this simplified model suitable to be employed for practical assessments of masonry walls subjected to rocking seismic failure mechanisms.

6. References

AlShawa O., Giresini L., Casapulla C. (2023). Comparison of the effects of traditional and innovative tie-rods in reducing the seismic vulnerability of church façades: the case of San Francesco in Mirandola (Italy), *Procedia Structural Integrity*, 44: 1364-1371.

Andreini M., De Falco A., Giresini L., Sassu M. (2013). Structural analysis and consolidation strategy of the historic Mediceo Aqueduct in Pisa (Italy), *Applied Mechanics and Materials*, 351-352: 1354-1357.

Caliò I., Marletta M., Pantò B. (2012). A new discrete element model for the evaluation of the seismic behaviour of unreinforced masonry buildings, *Engineering Structures*, 40: 327-338.

Casapulla C. (2001). Dry rigid block masonry: Safe solutions in presence of Coulomb friction, *WIT Transactions on the Built Environment*, 55: 251-261.

Casapulla C., Giresini L., Argiento L.U., Lagomarsino S. (2017). Analisi statiche e dinamiche incrementali per la valutazione della risposta fuori piano della facciata di una chiesa colpita dal terremoto centro-Italia 2016-17, *Proceedings of the XVII ANIDIS Conference on L'Ingegneria sismica in Italia*, Pistoia, Italy. [in Italian]

Casapulla C., Argiento L.U. (2016). The comparative role of friction in local out-of-plane mechanisms of masonry buildings. Pushover analysis and experimental investigation, *Engineering Structures*, 126: 158-173.

Casapulla C., Argiento L.U., Maione A., Speranza E. (2021). Upgraded formulations for the onset of local mechanisms in multi-storey masonry buildings using limit analysis, *Structures*, 31: 380-394.

Cattari S., Magenes G. (2021). Benchmarking the software packages to model and assess the seismic response of URM existing buildings through nonlinear analyses. *Bulletin of Earthquake Engineering*, 20: 1901-1936.

Chácara C., Cannizzaro F., Pantò B., Caliò I., Lourenço, P. B. (2019). Seismic vulnerability of URM structures based on a Discrete Macro-Element Modeling (DMEM) approach. *Engineering Structures*, 201: art. no. 109715.

Chen S., Bagi K. (2020). Crosswise tensile resistance of masonry patterns due to contact friction, *Proceedings of the Royal Society A: Mathematical, Physical and Engineering Sciences*, 476(2240): art. no. 20200439.

Coccia S., Como M. (2023). Out-of-plane dynamical strength of masonry walls under seismic actions, *Journal of Earthquake Engineering*, DOI: 10.1080/13632469.2023.2228913.

Cusmano V., Pantò B., Rapicavoli D., Caliò I. (2023). A discrete-element approach accounting for P-Delta effects, *Earthquake Engineering and Structural Dynamics*, 52: 2047–2066.

Degli Abbati S., Cattari S., Lagomarsino S. (2021). Validation of displacement-based procedures for rocking assessment of cantilever masonry elements, *Structures*, 33: 3397-3416.

Ferreira T.M., Costa A.A., Costa, A. (2015). Analysis of the out-of-plane seismic behavior of unreinforced masonry: A literature review, International Journal of Architectural Heritage, 9(8): 949-972.

Funari M.F., Pulatsu B., Szabó S., Lourenço P.B. (2022). A solution for the frictional resistance in macro-block limit analysis of non-periodic masonry, *Structures*, 43: 847–859.

Galvez F., Sorrentino L., Dizhur D., Ingham J.M. (2021). Using DEM to investigate boundary conditions for rocking urm façades subjected to earthquake motion, Journal of Structural Engineering, 147(11): art. no. 04021191.

Giresini L. (2022). Effect of dampers on the seismic performance of masonry walls assessed through fragility and demand hazard curves, *Engineering Structures*, 261: art. no. 114295.

Giresini L., Casapulla C., Croce P. (2021a). Environmental and economic impact of retrofitting techniques to prevent out-of-plane failure modes of unreinforced masonry buildings, *Sustainability*, 13(20): art. no. 11383.

Giresini L., Taddei F., Solarino F., Mueller G., Croce P. (2021b). Influence of stiffness and damping parameters of passive seismic control devices in one-sided rocking of masonry walls, *Journal of Structural Engineering (ASCE)*, 148(2): art. no. 04021257.

Heyman J. (1966). The stone skeleton, *International Journal of Solids and Structures*, 2(2): 249-279.

Jaimes M.A., Chávez M.M., Peña, F., Garcia Soto A. (2021). Out-of-plane mechanism in the seismic risk of masonry façades, *Bulletin of Earthquake Engineering*, 19: 1509–1535.

Ministero delle Infrastrutture e dei Trasporti – MIT (2019). *CNTC19-Circolare applicativa delle Norme Tecniche delle Costruzioni di cui al D.M. 17/01/2018 (NTC 2018)*. Gazzetta Ufficiale N. 42 del 20/02/2018. (in Italian)

Nale M., Benvenuti E., Chiozzi A., Minghini F., Tralli A. (2023). Effect of uncertainties on seismic fragility for out-of-plane collapse of unreinforced masonry walls, Journal of Building Engineering, 75, art. no. 106936.

Orosz Á., Bagi K. (2023). Comparison of contact treatment methods for rigid polyhedral discrete element models, *International Journal of Rock Mechanics and Mining Sciences*, 170: art. no. 105550.

Pantò B., Cannizzaro F., Caliò I., Lourenço P.B. (2017). Numerical and experimental validation of a 3D macro-model for the in-plane and out-of-plane behavior of unreinforced masonry walls, *International Journal of Architectural Heritage*, 11(7): 946-964.

Pepe M., Pingaro M., Trovalusci P., Reccia E., Leonetti L. (2020). Micromodels for the in-plane failure analysis of masonry walls: Limit analysis, FEM and FEM/DEM approaches, *Frattura ed Integrità Strutturale*, 14(51): 504-516.

Pulatsu B., Gencer F., Erdogmus E. (2022). Study of the effect of construction techniques on the seismic capacity of ancient dry-joint masonry towers through DEM, *European Journal of Environmental and Civil Engineering*, 26(9): 3913–3930.

Sorrentino L., AlShawa O., Decanini L.D. (2011). The relevance of energy damping in unreinforced masonry rocking mechanisms. Experimental and analytic investigations, *Bulletin of Earthquake Engineering*, 9: 1617–1642.

Sorrentino L., D'Ayala D., de Felice G., Griffith M.C., Lagomarsino S., Magenes G. (2017). Review of out-of-plane seismic assessment techniques applied to existing masonry buildings, *International Journal of Architectural Heritage*, 11(1): 2-21.

Szabó S., Funari M.F., Pulatsu B., Lourenço P.B. (2022). Lateral capacity of URM walls: a parametric study using macro and micro limit analysis predictions, *Applied Sciences*, 12(21): art. no. 10834.

Vadalà F., Cusmano V., Funari M.F., Caliò I., Lourenço P.B. (2022). On the use of a mesoscale masonry pattern representation in discrete macroelement approach, *Journal of Building Engineering*, 50: art. no. 104182.

Yavartanoo, F., Kang, T.H.-K. (2022). Dry-stack masonry wall modeling using finite-element method, *Journal of Structural Engineering (ASCE)*, 148(11): 04022176.